ECCOMAS Congress 2016
VII European Congress on Computational Methods in Applied Sciences and Engineering
M. Papadrakakis, V. Papadopoulos, G. Stefanou, V. Plevris (eds.)
Crete Island, Greece, 5–10 June 2016

HIGH-ORDER LINEARLY IMPLICIT TWO-STEP PEER METHODS FOR THE DISCONTINUOUS GALERKIN SOLUTION OF THE INCOMPRESSIBLE RANS EQUATIONS

Francesco Carlo Massa[2], Gianmaria Noventa[1], Francesco Bassi[2], Alessandro Colombo[2], Antonio Ghidoni[1] and Marco Lorini[1]

[1]Dipartimento di Ingegneria Meccanica e Inustriale, Universita degli Studi di Brescia
via Branze 38, 25123 Brescia, Italy
e-mail: {antonio.ghidoni, m.lorini006, g.noventa002}@unibs.it

[2] Dipartimento di Ingegneria Industriale, Universita degli studi di Bergamo
Viale Marconi 5, 24044 Dalmine (BG), Italy
e-mail: {francescocarlo.massa, francesco.bassi, alessandro.colombo}@unibg.it

Keywords: Discontinuous Galerkin discretization, linearly implicit Rosenbrock-type two-step peer methods, incompressible flows, unsteady simulations, NS, RANS, time-step adaptation strategy

Abstract. *In recent years the increasing attention to high-order Finite Volume (FV), Finite Element (FE) and spectral methods and the growth of computing power promote the development of high-order temporal schemes to perform robust, accurate and efficient unsteady long-time simulations. In this context, some features of the Discontinuous Galerkin finite element (DG) methods, e.g. compactness and flexibility, can be advantageous both for explicit and implicit time integration approaches. Explicit schemes can achieve very high accuracy, but are limited by time-step restrictions, while implicit schemes, even if memory consuming, can overcome time-step limitations, thus improving the time integration efficiency. During last decades several high order implicit temporal schemes have been developed, and some of them have been successfully coupled with DG methods. However these schemes can show the order reduction if applied to very stiff problems or problems with time-dependent boundary conditions. To overcome these limitations, high-order linearly implicit two-step peer methods have been proposed and successfully applied to the numerical solution of differential-algebraic equations. The aim of the present work is to implement high-order two-step peer methods in a DG code and assess their performance for the unsteady solution of the incompressible Navier-Stokes (INS) and Reynolds Averaged Navier-Stokes equations (RANS) equations.*

1 Introduction

In recent years, due to the increasing computational power and accuracy requirement, Discontinuous Galerkin (DG) method has become one of the most promising approaches to high-fidelity fluid dynamic computations in many technical areas, such as aeronautics, aeroacoustics and turbomachinery [17, 3, 2]. DG method proved to be very well suited for the Direct Numerical Simulation (DNS) [16, 15, 32] and the Large Eddy Simulation (LES) [31] of turbulent flows. Recently, the DG method has also been applied by Bassi *et al.* [3] to hybrid RANS-LES approaches in an attempt to overcome the poor predictive capabilities of the Reynolds-averaged Navier-Stokes (RANS) equations with first-moment closures in case of particular flow conditions, *e.g.*, massively separated flows.

These simulations require robust, accurate and efficient long time integration of unsteady flows, characterized by a wide range of temporal scales. Explicit schemes can achieve a very high accuracy [18, 19, 22] but are limited by time-step restriction. Otherwise, implicit schemes, although memory consuming due to the need of the Jacobian matrix, can be *A*-stable and *L*-stable even for high order of accuracy. Most popular implicit schemes are Backward Differentiation Formulae (BDF) [9], which are only *A*-stable up to the second-order, and their low accuracy is not well suited to match the spatial accuracy of DG methods. In the attempt to couple a high-order discretization both in space and time, several temporal schemes have been used to advance in time the DG space discretized equations [6, 26, 25, 5].

Among these schemes, Rosenbrock-type Runge-Kutta schemes [5] have received particular attention. In fact, being linearly implicit, they solve only one linear system per stage, showing a greater computational efficiency if compared to non linear methods [26, 25], which require to solve several non-linear systems at each time-step. Unfortunately, these Rosenbrock one-step methods can suffer from order reduction when they are applied to stiff problems. Additional order conditions can be derived to avoid the order reduction, but methods with higher order of convergence satisfying these conditions are difficult to find. For this reason, the class of the linearly implicit two-step peer methods [20] has been proposed for the numerical solution of time dependent Differential Algebric (DAE) and Partial Differential (PDE) equations. All solutions computed by Peer methods within a time-step have the same order of accuracy (this feature explains the attribute peer), and this is in contrast to one-step methods, where stage values have lower order than the final solution. Peer methods up to order eight are available in literature, and are characterized by good stability properties, *i.e.*, optimal zero-stability and $L\,(\alpha)$-stability [27], strong damping properties at infinity without further restrictions, and robustness with respect to stepsize changes. As all multi-step schemes, Peer methods are non self-starting and thus need a starting procedure in order to obtain required initial solutions. They are also multi-stage schemes and for each stage they require the solution of one linear system making them very attractive for practical computations. Since all stage solutions have the same accuracy and stability properties a continuous output of high-order is available with no extra-cost.

The aim of the present paper is to describe the implementation of high-order linearly implicit two-step peer methods in the DG MIGALE code for the integration in time of incompressible Navier-Stokes and RANS equations closed by the $k-\tilde{\omega}$ turbulence model [8]. Linearly implicit two-step peer methods up to sixth order of accuracy are assessed on two incompressible unsteady test cases: (i) the laminar travelling waves solution on a doubly periodic unit square domain and (ii) the turbulent flow around a circular cylinder for a Reynolds number $Re = 5 \times 10^4$. The travelling waves test case was used to investigate (i) the Peer methods order of accuracy, (ii) different types of starting procedure and their accuracy and (iii) the computational efficiency

of the schemes to obtain a given accuracy with the adaptive time-step strategy. Also the circular cylinder test case has been used to investigate the computational efficiency of Peer methods with the adaptive time-step strategy. A comparative assessment in terms of accuracy and performance with the traditional fourth order/six stages ESDIRK scheme [13] and third order/three stages (ROS3PL) [23] and fourth order/six stages (RODASP) [30] linearly implicit one-step Rosenbrock schemes has been done.

The paper is organized as follow: Section 2 describes the DG space discretization method for the Incompressible Navier-Stokes, RANS and turbulence model equations, while Section 3 introduces the class of the linearly implicit two-step peer methods and the adaptive time-step strategy. Numerical results are shown in Section 4, and the final Section 5 summarizes the results and presents the conclusion.

2 DG space discretization

Incompressible Navier-Stokes, RANS and turbulence model equations can be written in compact form as

$$\frac{\partial \widehat{\mathbf{q}}}{\partial t} + \nabla \cdot \mathbf{F}_c(\mathbf{q}) + \nabla \cdot \mathbf{F}_v(\mathbf{q}, \nabla \mathbf{q}) + \mathbf{s}(\mathbf{q}, \nabla \mathbf{q}) = \mathbf{0}, \tag{1}$$

where $\mathbf{q} \in \mathbb{R}^m$ denotes the vector of the m primitive variables $(p, u_i, k, \omega)^T$ (for $i = 1, d$), $\mathbf{s} \in \mathbb{R}^m$ the source term, d the space dimension. $\mathbf{F}_c, \mathbf{F}_v \in \mathbb{R}^m \otimes \mathbb{R}^d$ denote the inviscid and viscous flux functions, while $\widehat{\mathbf{q}} \in \mathbb{R}^m$ is defined as $(0, u_i, k, \omega)^T$.

To discretize the governing equations in space the system (1) is firstly multiplied by an arbitrary smooth test function $\mathbf{v} = \{v_1, \ldots, v_m\}$ and then integrated by parts, thus obtaining its weak form. The solution $\mathbf{q}$ and the test function $\mathbf{v}$ are then replaced with a finite element approximation $\mathbf{q}_h$ and a discrete test function $\mathbf{v}_h$ both belonging to $\mathbf{V}_h \stackrel{\text{def}}{=} [\mathbb{P}_d^k(\mathcal{T}_h)]^m$, where

$$\mathbb{P}_d^k(\mathcal{T}_h) \stackrel{\text{def}}{=} \left\{ v_h \in L^2(\Omega) \,|\, v_{h|K} \in \mathbb{P}_d^k(K),\ \forall K \in \mathcal{T}_h \right\} \tag{2}$$

is the discrete polynomial space in physical coordinates. $\mathbb{P}_d^k(K)$ denotes the restriction of the polynomial functions of d variables and total degree $\leq k$ to the element K belonging to the triangulation $\mathcal{T}_h = \{K\}$, consisting of a set of non-overlapping arbitrarily shaped and possibly curved elements, built on an approximation Ω_h of the domain Ω. We also define as $\mathcal{F}_h$ the set of the mesh faces $\mathcal{F}_h \stackrel{\text{def}}{=} \mathcal{F}_h^i \cup \mathcal{F}_h^b$, where $\mathcal{F}_h^b$ collects the faces located on the boundary of Ω_h. For any internal face $F \in \mathcal{F}_h^i$ there exist two elements $K^+, K^- \in \mathcal{T}_h$ such that $F \in \partial K^+ \cap \partial K^-$, where ∂ denotes cell boundaries. Moreover, for all $F \in \mathcal{F}_h^b$, $\mathbf{n}_F$ is the unit outward normal to Ω_h, whereas, for all $F \in \mathcal{F}_h^i$, $\mathbf{n}_F^-$ and $\mathbf{n}_F^+$ are the unit outward normals pointing to K^+ and K^-, respectively. To deal with discontinuous functions over the internal faces $F \in \mathcal{F}_h^i$ we introduce the jump $[\![\cdot]\!]$ and average $\{\cdot\}$ trace operators, that is

$$[\![v_h]\!] \stackrel{\text{def}}{=} v_{h|K^+}\mathbf{n}_F^+ + v_{h|K^-}\mathbf{n}_F^-, \qquad \{v_h\} \stackrel{\text{def}}{=} \frac{v_{h|K^+} + v_{h|K^-}}{2}. \tag{3}$$

When applied to vector functions these operators act componentwise.

Following the approach presented in [4], for each equation of the system, and without loss of generality, we choose the set of test and shape functions in any element K coincident with the set $\{\phi\}$ of N_{dof}^K orthogonal and hierarchical basis functions in that element. Such basis is

built by means of the modified Gram-Schmidt (MGS) algorithm, starting from a set of monomials defined over each elementary space $\mathbb{P}_d^k(K)$ in a reference frame relocated in the element barycenter and aligned with the principal axes of inertia of K.

Each component $q_{h,j}$, $j = 1, \ldots, m$, of the numerical solution $\mathbf{q}_h \in \mathbf{V}_h$ can be expressed, in terms of the elements of the global vector $\mathbf{Q}$ of unknown degrees of freedom, as $q_{h,j} = \phi_l Q_{j,l}$, $l = 1, \ldots, N_{dof}^K$, $\forall K \in \mathcal{T}_h$.

Accounting for these aspects, the DG discretization of the RANS and turbulence model equations consists in seeking, for $j = 1, \ldots, m$, the elements of $\mathbf{Q}$ such that

$$\sum_{K\in\mathcal{T}_h} \int_K \phi_i \phi_l \frac{dQ_{k,l}}{dt} d\mathbf{x} - \sum_{K\in\mathcal{T}_h} \int_K \frac{\partial \phi_i}{\partial x_n} F_{j,n}\left(\mathbf{q}_h, \nabla_h \mathbf{q}_h + \mathbf{r}\left([\![\mathbf{q}_h]\!]\right)\right) d\mathbf{x} + \sum_{F\in\mathcal{F}_h} \int_F [\![\phi_i]\!]_n \widehat{F}_{j,n}\left(\mathbf{q}_h^{\pm}, \left(\nabla_h \mathbf{q}_h + \eta_F \mathbf{r}_F\left([\![\mathbf{q}_h]\!]\right)\right)^{\pm}\right) d\sigma + \sum_{K\in\mathcal{T}_h} \int_K \phi_i s_j\left(\mathbf{q}_h, \nabla_h \mathbf{q}_h + \mathbf{r}\left([\![\mathbf{q}_h]\!]\right)\right) d\mathbf{x} = 0, \quad (4)$$

for $i = 1, \ldots, N_{dof}^K$ and where repeated indices imply summation over the ranges $k = 1, \ldots, m$, $l = 1, \ldots, N_{dof}^K$ and $n = 1, \ldots, d$.

In Eq. (4) $\mathbf{F}$ denotes the sum of the convective and viscous flux functions, and $\widehat{\mathbf{F}}$ the sum of their numerical counterparts. For the former the flux computation is based on the exact solution of the Riemann problem for the artificial compressibility perturbation of the locally 1D inviscid Euler equations, as suggested in [7, 8], while for the latter the BR2 scheme is employed, proposed in [9] and theoretically analyzed in [11, 1].

3 Time discretization

The discrete problem corresponding to Eq. (4) can be written as:

$$\widehat{\mathbf{M}} \frac{d\mathbf{Q}}{dt} + \mathbf{R}\left(\mathbf{Q}\right) = \mathbf{0}, \quad (5)$$

where $\mathbf{Q}$ is the global vector of unknown degrees of freedom, $\mathbf{R}$ the residuals vector, and $\widehat{\mathbf{M}}$ the global block diagonal mass matrix. Thanks to the use of orthonormal base functions defined in physical space, the matrix $\widehat{\mathbf{M}}$ is simply the identity matrix with null entries corresponding to the pressure degrees of freedom due to the lack of pressure time derivatives.

In this work the Eq. (5) is advanced in time in an implicit sense, by using the high-order linearly implicit two-step peer methods.

3.1 Linearly implicit two-step peer methods

The s-stage linearly implicit two-step peer method computes solution approximations $\mathbf{Q}_i^n$, $i = 1, \ldots, s$, of the Eq. (5) at times $t_i^n = t^n + c_i \Delta t^n$ by means of s linear systems:

$$\left(\frac{\widehat{\mathbf{M}}}{\gamma \Delta t^n} + \mathbf{J}_s^{n-1}\right)\left(\mathbf{Q}_i^n - \mathbf{Q}_{0i}^{\ n}\right) = -\mathbf{R}_{0i}^{\ n} + \frac{\widehat{\mathbf{M}}}{\gamma \Delta t^n}\left(\mathbf{Y}_i - \mathbf{Q}_{0i}^{\ n}\right) \qquad i = 1, ..., s, \quad (6)$$

where

$$\mathbf{Y}_i = \sum_{j=1}^{i-1} \frac{a_{ij}}{\gamma}\left(\mathbf{Q}_j^n - \mathbf{Y}_j\right) + \sum_{j=1}^{s} u_{ij} \mathbf{Q}_j^{n-1}, \quad (7)$$

$$\mathbf{Q}_{0_i}^{\ n} = \sum_{j=1}^{i-1} \frac{a_{0ij}}{\gamma} \left(\mathbf{Q}_j^n - \mathbf{Y}_j \right) + \sum_{j=1}^{s} u_{0ij} \mathbf{Q}_j^{n-1}, \tag{8}$$

with

$$\mathbf{J}_s^{n-1} = \frac{\partial \mathbf{R}(\mathbf{Q}_s^{n-1})}{\partial \mathbf{Q}}, \tag{9}$$

At each step, an embedded solution can be computed as

$$\hat{\mathbf{Q}}_s^{\ n} = \sum_{i=1}^{s-1} \alpha_i \mathbf{Q}_i^n. \tag{10}$$

$\mathbf{A} = \{a_{ij}\}$, $\mathbf{U} = \{u_{ij}\}$, $\mathbf{A}_0 = \left\{a_{0ij}\right\}$ and $\mathbf{U}_0 = \left\{u_{0ij}\right\}$ are $s \times s$ matrices of real coefficients and α_i, c_i and γ are real parameters. $\mathbf{U}$ and $\mathbf{U}_0$ depend on the step size ratio $\sigma^n = \Delta t^n / \Delta t^{n-1}$ between current and previous steps in order to ensure accuracy and stability properties for variable step sizes.

The Jacobian matrix of the DG space discretization $\mathbf{J}_s^{n-1}$ is computed only once per step with the last stage solution $\mathbf{Q}_s^{n-1}$ of the previous step. Thanks to the peculiar treatment of the convective numerical flux, $\mathbf{J}_s^{n-1}$ has non null entries for pressure degrees of freedom; it follows that, despite the singularity of matrix $\widehat{\mathbf{M}}$, Eq. (6) can be solved with standard algorithms.

In order to compute step $n = 1$ of the two-step method described in Eq. (6), initial solutions $\mathbf{Q}_i^0$, $i = 1, \ldots, s$, at times $t_i^0 = t^{st} + c_i \Delta t^{st}$ must be available, where superscript st denotes the starting step. The initialization algorithm to compute $\mathbf{Q}_i^0$ will be described in Sec. 3.3.

3.2 Accuracy and stability properties

Matrices $\mathbf{A}$, $\mathbf{U}$, $\mathbf{A}_0$ and $\mathbf{U}_0$ and parameters γ and c_i uniquely define accuracy and stability properties of a s-stage Peer method. Consistency and zero stability conditions that ensure order $q = s - 1$ for all step size ratio $\sigma > 0$ and for all Peer stages are provided in [27, 20]; it follows that all quantities computed by Eqs. (6), (7) and (8) have the same accuracy and stability properties. Furthermore, these conditions are derived independently from the Jacobian matrix, which thus can be computed numerically, e.g. by means of finite differences. As proposed in Ref. [27], matrices $\mathbf{A}$, $\mathbf{U}$, $\mathbf{A}_0$ and $\mathbf{U}_0$ are functions of parameters c_i and γ, and coefficients c_i are chosen to be stretched Chebychev nodes in the interval $[-1, 1]$:

$$c_i = -\frac{\cos\left(\left(i - \frac{1}{2}\right)\frac{\pi}{s}\right)}{\cos\left(\frac{\pi}{2s}\right)}, \qquad i = 1, \ldots, s. \tag{11}$$

The γ parameter specifies the θ angle of $A\,(\theta)$- and $L\,(\theta)$-stability, and, as demonstrated in [27], can guarantees (if conveniently chosen) an order $q = s$ for a s-stage Peer method. with constant time-step. Finally, coefficients α_i, $i = 1, \ldots, s - 1$, are only function of nodes c_i,and are computed such that the order of the embedded solution is equal to $\hat{q} = s - 2$ (see Ref. [20]).

Peer methods implemented have three, four, five and six stages and in this work are referred as peer3A, peer4A, peer5A and peer6A. They are A-stable and L-stable, *i.e.* $\theta = 90$, and have order $q = s - 1$ and $q = s$ for variable and constant time-step, respectively. The γ values adopted for each scheme are reported in Tab. 1.

Table 1: List of γ values and corresponding θ angles of $A(\theta)$-stability and $L(\theta)$-stability for each Peer method used in this work.

	s	γ	θ
peer3A	3	$2.165162598341552E+00$	90
peer4A	4	$1.038881828680110E+00$	90
peer5A	5	$5.614731292097847E-01$	90
peer6A	6	$3.476356828221134E-01$	90

3.3 Starting procedure

Peer methods are multi-step and multi-stage time integration schemes. As all multi-step schemes, they are not self-starting, that means they need a set of starting solutions $\mathbf{Q}_i^0$ at times:

$$t_i^0 = t^{st} + c_i \Delta t^{st}, \qquad i = 1, \dots, s \tag{12}$$

where

$$\Delta t^{st} = t^1 - t^{st}, \tag{13}$$

in order to perform the first step $n = 1$.

Defining

$$c^- = \min_{i \in [1,s]} (c_i), \qquad t^- = t^{st} + c^- \Delta t^{st} \tag{14}$$

as the minimum value of nodes c_i and the smallest time point of the starting procedure, respectively, and imposing that t^- is equal to initial time t^0, it follows from Eqs. (12) and (13) that:

$$t_i^0 = t^0 + \left(c_i - c^-\right) \Delta t^{st}, \qquad i = 1, \dots, s, \tag{15}$$

$$t^1 = t^0 + \left(1 - c^-\right) \Delta t^{st}, \tag{16}$$

where Δt^{st} is the starting procedure time-step here imposed equal to the user-defined initial time-step of Peer methods,

$$\Delta t^{st} = \Delta t^1, \tag{17}$$

in order to ensure $\sigma^1 = 1$.

Starting solutions at corresponding times t_i^0 can be obtained by means of a one-step time integration scheme, *e.g.* Rosenbrock or ESDIRK scheme. It is mandatory that the accuracy of $\mathbf{Q}_i^0$ is proportional to the accuracy of the Peer method used for the simulation, otherwise a reduction of the accuracy order is introduced. Basing on the asymptotic behaviour of time integration errors, this request leads to:

$$T^{st} \left(\overline{\Delta t'}\right)^{q'} \propto \left(\overline{\Delta t}\right)^{q}, \tag{18}$$

where $\overline{\Delta t'}$ and $\overline{\Delta t}$ are the mean time-steps used by the one-step scheme of order q' and Peer method of order q, respectively and T^{st} is the starting procedure period that can be computed from Eq. (15) as:

$$T^{st} = \left(c^+ - c^-\right) \Delta t^{st}, \tag{19}$$

with $c^+ = \max_{i \in [1,s]} (c_i)$. Since $\overline{\Delta t} \propto \Delta t^1$, from Eq. (17) it follows that:

$$\overline{\Delta t'} = \psi \left(\Delta t^1\right)^{\frac{q-1}{q'}}, \tag{20}$$

where the constant value must be defined by the user. For simplicity we consider $\psi = 1$. After sorting the starting time points such that:

$$t_j^0 < t_{j+1}^0, \qquad j = 1, \ldots, s-1, \tag{21}$$

with in general $t_j^0 \neq t_i^0$, it can be found the number of steps,

$$N_j' = \text{int}\left[\frac{\left(t_{j+1}^0 - t_j^0\right)}{\left(\overline{\Delta t'}\right)}\right] + 1, \tag{22}$$

needed to integrate in time from t_j^0 to t_{j+1}^0 by means of the one-step scheme and, as a consequence, the corresponding fixed time-step:

$$\Delta t'_j = \frac{\left(t_{j+1}^0 - t_j^0\right)}{N_j'}. \tag{23}$$

Notice that $\Delta t'_j \leq \overline{\Delta t'}$. Finally, starting from $\mathbf{Q}_j^0$, the solution $\mathbf{Q}_{j+1}^0$ can be achieved after N_j' steps of dimension $\Delta t_j'$ performed with a one-step temporal scheme.

3.4 Time-step adaptation algorithm

The time-step control is an important feature to increase the efficiency and robustness of a time integration method. The adaptive technique is based on the local error estimator, which exploit the lower order embedded solution to approximate the local truncation error of the considered temporal scheme:

$$r^{n+1} = \frac{\|\mathbf{Q}^n - \hat{\mathbf{Q}^n}\|_2}{d}, \tag{24}$$

where d is the threshold tolerance, defined as:

$$d = ATOL + RTOL\|\mathbf{Q}^n\|_2. \tag{25}$$

with $ATOL$ and $RTOL$ user-defined absolute and relative tolerances, respectively. In this work is set $ATOL = RTOL = TOL$, that leads to:

$$d = TOL + TOL\|\mathbf{Q}^{n+1}\|_2. \tag{26}$$

Considering relations proposed by Söderlind et al., in [28, 29], the next time-step Δt^{n+1} can be computed as:

$$\Delta t^{n+1} = \min\left(\left(1 + 2\text{atan}\left[\left(\rho^n - 1\right)/2\right]\right)\Delta t^n, \Delta t_{max}\right), \tag{27}$$

where

$$\rho^n = \left(\frac{\Delta t^n}{\Delta t^{n-1}}\right)^{-\alpha_2}\left(\frac{1}{r^{n+1}}\right)^{\beta_1}\left(\frac{1}{r^n}\right)^{\beta_2}, \tag{28}$$

$\hat{q}\beta_1 = \hat{q}\beta_2 = \alpha_2 = 1/4$, Δt^n is the current time-step, Δt^{n-1} the previous time-step, $\hat{q}$ the order of the embedded scheme, r^n the previous local error estimator and Δt_{max} the user-defined maximum allowable time-step which can be defined as a fraction of the characteristic temporal scale of the considered flow problem (*e.g.* the vortex shedding period).

If $r_{n+1} > \delta$, the current time-step Δt^n is rejected and the iteration recomputed with Δt^{n+1}. $\delta > 1$ is a user-defined safety factor, here set to 1.5.

The time-step adaptation algorithm should operate in a tolerance proportional mode, *i.e.* a change of the user defined tolerance TOL by one order of magnitude should correspond to a change of the solution error by one order of magnitude. Furthermore, the different time integration schemes should deliver the same accuracy for the same tolerance setting. These features can be obtained with a proper scaling and calibration of the adaptation algorithm by using a modified input tolerance TOL' inside Eq. (26), where:

$$TOL' = \beta TOL_0^{(k-1)/k} TOL^{1/k}. \tag{29}$$

TOL_0 is the equivalence point determined during the calibration, β is a constant to have similar accuracies for the same TOL and different time integration schemes at the end of the simulations and k is the measured order of the curve $error - TOL'$ of the reference computations used for the calibration. The calibration was done on the travelling waves test case (see Section 4.1), where the analytical solution is known, and on the circular cylinder (see Section 4.2), computing a reference solution [29].

Finally, the tolerance of the iterative method used for the solution of linear systems (6) is set as

$$TOL_{GMRES} = \eta TOL', \tag{30}$$

where η is a safety factor. The choice of η will be numerically investigated in the Section 4.1.

4 Results

In this section the robustness and the accuracy of the proposed coupling between high-order DG method and high-order linearly implicit two-step peer schemes are demonstrated by means of the analysis of two incompressible test cases.

The first test case is the laminar solution of travelling dumped waves on a doubly periodic unit square domain. In the second test case, the unsteady turbulent flow around a circular cylinder is performed for $Re = 5 \times 10^4$ based on the circle diameter and on the freestream conditions [10]. The convergence order of Peer temporal schemes up to six stages, the correctness of the starting procedure and the influence of the system tolerance TOL_{System} have been assessed for the laminar test case. Afterwards, the efficiency of the proposed DG-Peer coupling was investigated for a turbulent test case by means of the adaptive time-step strategy and compared with the traditional one-step temporal schemes, *i.e.* the fourth order/six stages ESDIRK scheme [13] and the third order/three stages (ROS3PL) [23] and fourth order/six stages (RODASP) [30] linearly implicit one-step Rosenbrock schemes.

Computations have been run on a Linux cluster with 12 AMD 6220 CPUs (8 cores per CPU). Computing times t_{CPU} reported in this work are normalized values with respect to the *TauBenchmark* [12] value, $t_{TauBench}$, obtained on a full node of the cluster used for the CFD simulation[1]. The normalized computing time is measured as work units (wu) and is defined as wu=$(t_{CPU} n_{cores})/t_{TauBench}$, where t_{CPU} is the wall clock time and n_{cores} the numbers of cores.

[1] -n 250000 -s 10 define the reference TauBench workload for the hardware benchmark.

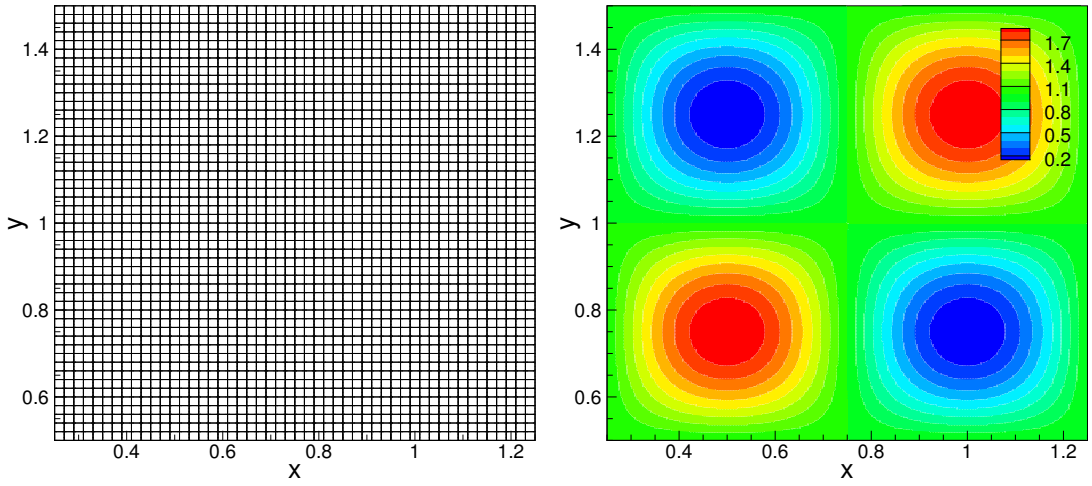

Figure 1: Travelling waves. Computational mesh (left), 2500 quadrilateral elements with linear edges, and velocity (x-component) contours after a simulation time $\Delta t_{sim} = T$ (right), $\mathbb{P}^6$ solution approximation

4.1 Travelling waves

The analytical solution of the laminar travelling dumbed waves test case is defined as:

$$u_1(x,y,t) = 1 + 2\cos(2\pi(x-t))\sin(2\pi(y-t))\,e^{-8\pi^2\nu t}, \tag{31}$$

$$u_2(x,y,t) = 1 - 2\sin(2\pi(x-t))\cos(2\pi(y-t))\,e^{-8\pi^2\nu t}, \tag{32}$$

$$p(x,y,t) = -(\cos(4\pi(x-t)) + \cos(4\pi(y-t)))\,e^{-16\pi^2\nu t}, \tag{33}$$

with $\nu = 1\mathrm{e}{-2}$. The domain is the doubly periodic unit square $[0.25, 1.25] \times [0.5, 1.5]$. A $\mathbb{P}^6$ solution approximation is used to keep the space discretization error below the time integration error (see Fig. 1 for the mesh and the velocity contours). The time integration period T is set equal to one non-dimensional convective time.

The convergence order of Peer schemes has been first verified, considering the following time-steps: $T/40$, $T/80$, $T/160$, $T/320$ and $T/400$ and a system tolerance $TOL_{GMRES} = 10^{-15}$. All schemes verify the expected convergence order $q = s$ for constant stepsize, as shown in Tab. 2. The errors of peer6A at smallest time-steps are affected by the machine error, thus preventing the verification of the convergence order. The initial solution $\mathbf{Q}_i^0$ is simply defined by the analytical solution of the problem at times $t^0_{i=1,\dots,s}$.

In general, the analytical solution is not available and starting values $\mathbf{Q}^0_{i=1,\dots,s}$ must be computed numerically by means of one-step time integration schemes. The starting procedure described in Section 3.3 is here tested adopting linearly-implicit Rosenbrock-type Runge-Kutta schemes ROS3PL [23] ($q' = 3$), RODASP [30] ($q' = 4$) and RODAS-ROD5_1 [24] ($q' = 5$). In particular, higher order RODASP and RODAS-ROD5_1 schemes are used only for peer5A and peer6A, respectively, while lower order ROS3PL is applied to all Peer methods.

Tab. 3 shows the L^2 norm of the pressure error ($\|err_p\|_2$) and the computational time obtained with numerical starting procedure. It can be seen that the Peer methods order of convergence is preserved. However, using a low order one-step scheme, *i.e.* ROS3PL, to initialize a high order Peer method is not efficient because the time-step needed by the one-step method to preserve the order of the Peer methods is too small.

The parameter η, used in Eq. (30), has been first chosen for each schemes with the adaptive time-step strategy, in order to set the system tolerance TOL_{GMRES} as a function of the adaptive

Table 2: Travelling waves. L^2 norm of the pressure ($\|err_p\|_2$) and velocity components ($\|err_u\|_2$, $\|err_v\|_2$) errors, and convergence order for Peer schemes with exact initialization, $\mathbb{P}^6$ solution approximation

	Δt	CFL	$\|err_p\|_2$	order	$\|err_u\|_2$	order	$\|err_v\|_2$	order
	T/40	7.96	1.78E-01	1.57	2.76E-01	1.57	2.76E-01	1.57
	T/80	3.98	3.74E-02	2.92	5.82E-02	2.92	5.82E-02	2.92
peer3A	T/160	1.99	4.84E-03	2.98	7.54E-03	2.98	7.54E-03	2.98
	T/320	1.00	6.13E-04	2.99	9.54E-04	2.99	9.54E-04	2.99
	T/400	0.80	3.15E-04	-	4.90E-04	-	4.90E-04	-
	T/40	7.96	8.53E-03	3.74	1.33E-02	3.73	1.33E-02	3.73
	T/80	3.98	6.01E-04	3.93	9.36E-04	3.93	9.36E-04	3.93
peer4A	T/160	1.99	3.88E-05	3.98	6.04E-05	3.98	6.04E-05	3.98
	T/320	1.00	2.45E-06	3.99	3.82E-06	3.99	3.82E-06	3.99
	T/400	0.80	1.01E-06	-	1.57E-06	-	1.57E-06	-
	T/40	7.96	2.75E-04	4.89	4.28E-04	4.89	4.28E-04	4.89
	T/80	3.98	9.07E-06	4.97	1.41E-05	4.97	1.41E-05	4.97
peer5A	T/160	1.99	2.87E-07	4.99	4.47E-07	4.99	4.47E-07	4.99
	T/320	1.00	9.02E-09	5.00	1.40E-08	5.00	1.40E-08	5.00
	T/400	0.80	2.96E-09	-	4.60E-09	-	4.60E-09	-
	T/40	7.96	7.66E-06	5.98	1.19E-05	5.98	1.19E-05	5.98
	T/80	3.98	1.20E-07	6.01	1.86E-07	6.01	1.86E-07	6.01
peer6A	T/160	1.99	1.87E-09	5.80	2.89E-09	6.03	2.89E-09	6.03
	T/320	1.00	1.78E-10	-	4.06E-11	-	4.06E-11	-
	T/400	0.80	1.76E-10	-	1.81E-11	-	1.81E-11	-

Table 3: Travelling waves. L^2 norm of the pressure ($\|err_p\|_2$) error, convergence order and computational time for Peer schemes with numerical starting procedure, $\mathbb{P}^6$ solution approximation

	Δt	CFL	$\|err_p\|_2$	order	$\|err_u\|_2$	order	$\|err_v\|_2$	order	CPU time [wu]
	T/40	7.96	1.78E-01	1.57	2.76E-01	1.57	2.76E-01	1.57	2.66E+03
	T/80	3.98	3.74E-02	2.92	5.82E-02	2.92	5.82E-02	2.92	3.02E+03
peer3A (ROS3PL)	T/160	1.99	4.84E-03	2.98	7.54E-03	2.98	7.54E-03	2.98	3.88E+03
	T/320	1.00	6.13E-04	2.99	9.54E-04	2.99	9.54E-04	2.99	5.58E+03
	T/400	0.80	3.15E-04	-	4.90E-04	-	4.90E-04	-	6.55E+03
	T/40	7.96	8.52E-03	3.74	1.33E-02	3.73	1.33E-02	3.73	1.78E+03
	T/80	3.98	6.01E-04	3.93	9.35E-04	3.93	9.35E-04	3.93	2.22E+03
peer4A (ROS3PL)	T/160	1.99	3.88E-05	3.98	6.04E-05	3.98	6.04E-05	3.98	3.28E+03
	T/320	1.00	2.45E-06	3.99	3.81E-06	3.99	3.81E-06	3.99	6.16E+03
	T/400	0.80	1.01E-06	-	1.57E-06	-	1.57E-06	-	7.15E+03
	T/40	7.96	2.75E-04	4.89	4.29E-04	4.89	4.29E-04	4.89	1.60E+03
	T/80	3.98	9.07E-06	4.97	1.41E-05	4.97	1.41E-05	4.97	2.14E+03
peer5A (RODASP)	T/160	1.99	2.87E-07	4.99	4.47E-07	4.99	4.47E-07	4.99	3.62E+03
	T/320	1.00	9.02E-09	5.00	1.40E-08	5.00	1.40E-08	5.00	6.03E+03
	T/400	0.80	2.96E-09	-	4.60E-09	-	4.60E-09	-	7.63E+03
	T/40	7.96	2.75E-04	4.89	4.29E-04	4.89	4.29E-04	4.89	1.54E+03
	T/80	3.98	9.08E-06	4.97	1.41E-05	4.97	1.41E-05	4.97	2.25E+03
peer5A (ROS3PL)	T/160	1.99	2.87E-07	4.99	4.48E-07	4.99	4.48E-07	4.99	3.89E+03
	T/320	1.00	9.03E-09	4.99	1.41E-08	5.00	1.41E-08	5.00	7.50E+03
	T/400	0.80	2.96E-09	-	4.61E-09	-	4.61E-09	-	7.78E+03
	T/40	7.96	7.66E-06	5.98	1.19E-05	5.98	1.19E-05	5.98	1.66E+03
	T/80	3.98	1.20E-07	6.01	1.86E-07	6.01	1.86E-07	6.01	2.24E+03
peer6A (ROD5_1)	T/160	1.99	1.87E-09	5.80	2.89E-09	6.03	2.89E-09	6.03	3.81E+03
	T/320	1.00	1.78E-10	-	4.06E-11	-	4.06E-11	-	6.16E+03
	T/400	0.80	1.79E-10	-	1.81E-11	-	1.81E-11	-	6.75E+03
	T/40	7.96	7.65E-06	5.99	1.19E-05	5.98	1.19E-05	5.98	2.32E+03
	T/80	3.98	1.20E-07	6.00	1.86E-07	6.00	1.86E-07	6.00	4.72E+03
peer6A (ROS3PL)	T/160	1.99	1.86E-09	5.79	2.89E-09	6.02	2.89E-09	6.02	9.03E+03
	T/320	1.00	1.79E-10	-	4.05E-11	-	4.05E-11	-	1.98E+04
	T/400	0.80	1.74E-10	-	1.80E-11	-	1.80E-11	-	2.42E+04

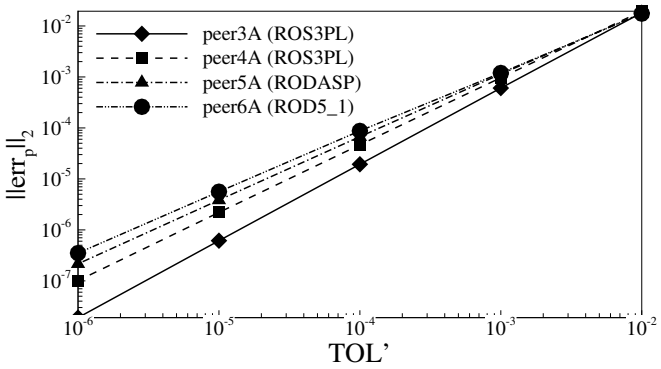

Figure 2: Travelling waves. L^2 norm of the pressure error ($\|err_p\|_2$) as a function of the adaptive tolerance TOL' for adaptive Peer schemes, $TOL_{GMRES} = 10^{-15}$ and $\mathbb{P}^6$ solution approximation

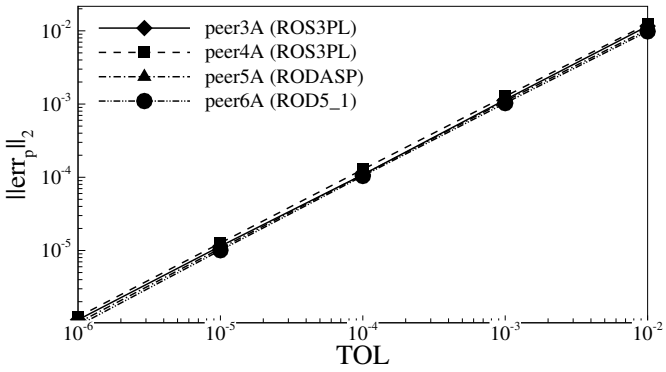

Figure 3: Travelling waves. L^2 norm of the pressure error ($\|err_p\|_2$) as a function of the user defined tolerance TOL for adaptive Peer schemes, $TOL_{GMRES} = \eta TOL$ and $\mathbb{P}^6$ solution approximation

tolerance TOL'. The results, summarized in Tab. 4, show the different errors with respect to the reference solution with $TOL_{GMRES} = 10^{-15}$. The pressure error starts to change only when $TOL_{GMRES} \geq 0.1\,TOL'$, that leads to set $\eta = 0.1$.

Fig. 2 shows the L^2 norm of the pressure error ($\|err_p\|_2$) as a function of the adaptive tolerance TOL'. Without scaling procedure and for a given tolerance TOL', the adaptive time-step strategy provides different errors for different Peer methods. However, the tolerance calibration defined by Eq. (29) allows to achieve the same error for different Peer schemes, as shown in Fig. 3. After the calibration each scheme shows comparable errors for the same user defined tolerance TOL. Tab. 5 summarizes the parameters of the calibration procedure.

Fig. 4 compare the performance of the Peer methods with the one-step traditional methods. The efficiency of the Peer methods increases with the order of convergence. The performance of peer6A and peer5A is comparable with RODASP scheme and peer4A with ROS3PL scheme. Only peer3A achieves a low computational efficiency.

4.2 Turbulent flow around a circular cylinder

The coupling between DG method and Peer schemes has been investigated also computing the turbulent flow around a circular cylinder for a Reynolds number $Re = 5 \times 10^4$, based on the cylinder diameter and the freestream conditions.

The far-field boundary is at 50 chords from the circle and the first cell height is equivalent to $y^+ \sim 4$ (see Fig. 5 for the mesh and Fig. 6 for the pressure and turbulent intensity contours).

Table 4: Travelling waves. Average time-step Δt_{avg} and Courant-Friedrichs-Lewy number CFL_{avg}, L^2 norm of the pressure ($\|err_p\|_2$) and velocity components ($\|err_u\|_2$, $\|err_v\|_2$) errors and the computational time for adaptive Peer schemes and different system tolerances TOL_{GMRES}, $TOL' = 10^{-3}$ and $\mathbb{P}^6$ solution approximation

	TOL_{GMRES}	Δt_{avg}	CFL_{avg}	$\|err_p\|_2$	$\|err_u\|_2$	$\|err_v\|_2$	CPU time [wu]
peer3A (ROS3PL)	1.00E-06	3.06E-03	0.97	6.05E-04	9.42E-04	9.42E-04	3.67E+03
	1.00E-05	3.06E-03	0.97	6.05E-04	9.42E-04	9.42E-04	3.28E+03
	1.00E-04	3.06E-03	0.97	6.00E-04	9.35E-04	9.35E-04	2.47E+03
	1.00E-03	3.06E-03	0.97	5.89E-04	9.13E-04	9.14E-04	2.14E+03
	1.00E-02	3.06E-03	0.97	5.89E-04	9.13E-04	9.14E-04	2.08E+03
	1.00E-01	3.05E-03	0.91	2.69E-03	4.23E-03	4.23E-03	1.76E+03
peer4A (ROS3PL)	1.00E-06	1.37E-02	4.36	9.66E-04	1.50E-03	1.50E-03	1.32E+03
	1.00E-05	1.37E-02	4.36	9.66E-04	1.50E-03	1.50E-03	1.10E+03
	1.00E-04	1.37E-02	4.36	9.66E-04	1.50E-03	1.50E-03	9.88E+02
	1.00E-03	1.37E-02	4.36	9.78E-04	1.52E-03	1.52E-03	8.51E+02
	1.00E-02	1.39E-02	4.42	1.24E-03	1.98E-03	1.98E-03	6.52E+02
	1.00E-01	5.92E-03	1.88	7.89E-03	8.46E-03	7.41E-03	1.71E+03
peer5A (RODASP)	1.00E-06	3.23E-02	10.28	1.14E-03	1.78E-03	1.78E-03	7.48E+02
	1.00E-05	3.23E-02	10.28	1.14E-03	1.78E-03	1.78E-03	6.73E+02
	1.00E-04	3.23E-02	10.28	1.14E-03	1.78E-03	1.78E-03	5.69E+02
	1.00E-03	3.23E-02	10.28	1.13E-03	1.77E-03	1.77E-03	4.50E+02
	1.00E-02	3.23E-02	10.28	1.21E-03	1.62E-03	1.71E-03	3.67E+02
peer6A (ROD5_1)	1.00E-06	5.56E-02	17.70	1.20E-03	1.86E-03	1.86E-03	6.24E+02
	1.00E-05	5.56E-02	17.70	1.20E-03	1.86E-03	1.86E-03	5.09E+02
	1.00E-04	5.56E-02	17.70	1.20E-03	1.87E-03	1.87E-03	4.49E+02
	1.00E-03	5.26E-02	16.77	9.75E-04	1.71E-03	1.94E-03	5.27E+02

Table 5: Travelling waves. Parameters for the calibration procedure

	k	β	TOL_0
peer3A	1.49	5.16	10^{-4}
peer4A	1.32	2.14	10^{-4}
peer5A	1.23	1.49	10^{-4}
peer6A	1.17	1.14	10^{-4}

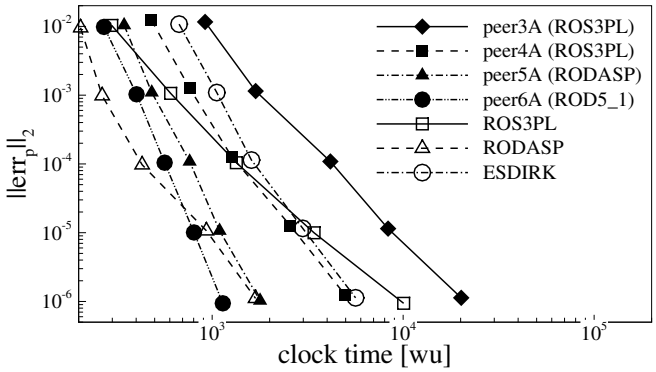

Figure 4: Travelling waves. L^2 norm of the pressure error ($\|err_p\|_2$) as a function of the computational time for adaptive Peer schemes, $TOL_{GMRES} = \eta\, TOL$ and $\mathbb{P}^6$ solution approximation

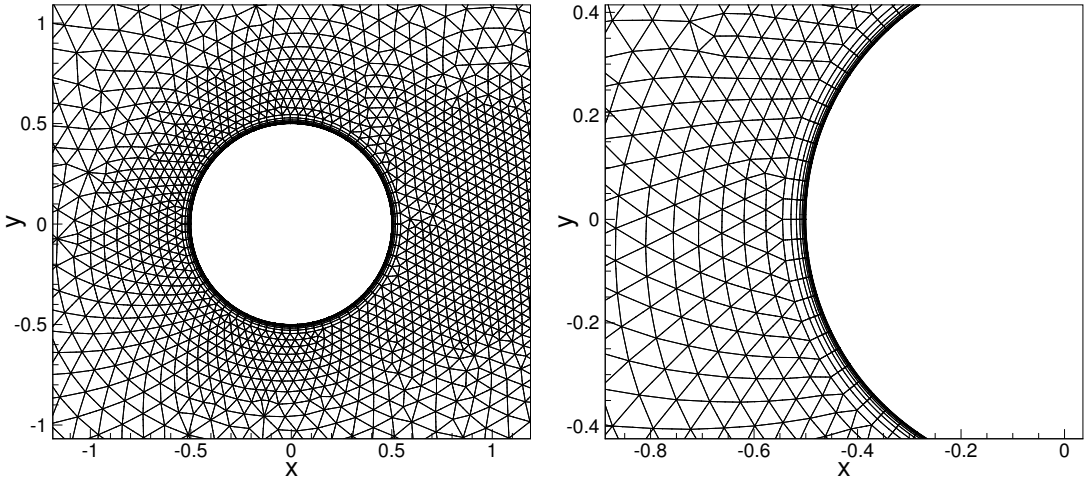

Figure 5: Cylinder. Computational mesh (left) of a circular cylinder, 8753 quadratic elements, and detail of the boundary layer (right)

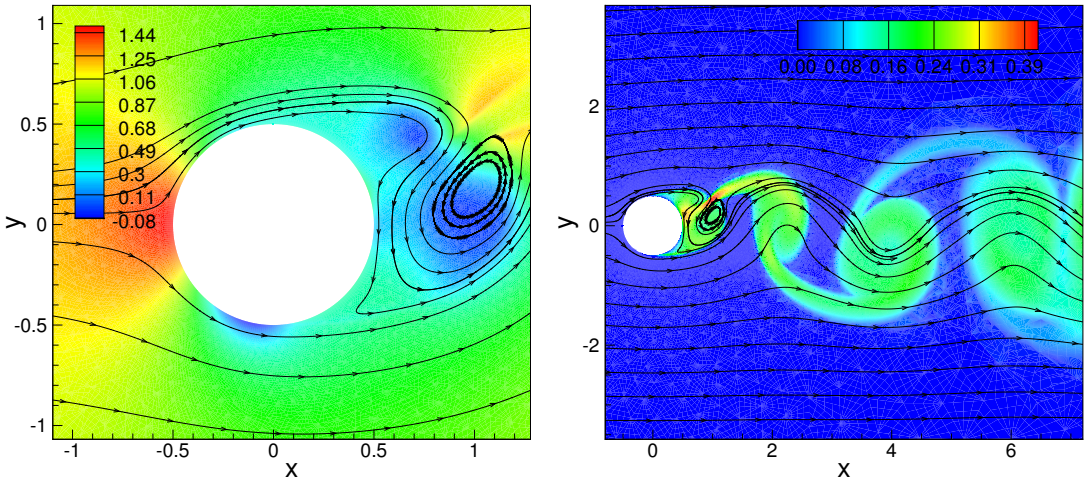

Figure 6: Cylinder. Pressure (left) and turbulence intensity (right) contours, $\mathbb{P}^3$ solution approximation

A $\mathbb{P}^3$ solution approximation provides a number of DOF, 87530, comparable with the computations on a fine mesh proposed by Carpenter *et. al.* on the same test case with a Finite Volume code [14]. The grid has been generated with a $2D$ high-order version of a fully automated in-house hybrid mesh generator based on the Advancing-Delaunay strategy [21].

Time integration error has been computed using the error of the lift coefficient:

$$err_{C_L} = C_L - C_{L,ref}. \tag{34}$$

The time integration period is set equal to one forth of the vortex shedding period. All computations start from the same initial flow field and the reference solution and the $C_{L,ref}$ have been obtained with the RODASP scheme and the following parameters for the adaptive time-step strategy: $TOL' = 10^{-9}$, $TOL_{GMRES} = \eta TOL'$.

The convergence order analysis has not been considered for this test case, due to the not optimal convergence results shown by Carpenter *et. al.* [14], which will certainly characterize also the schemes investigated in this work. Simulations have been carried out only with the adaptive time-step strategy and for the starting procedure the following one-step time integration

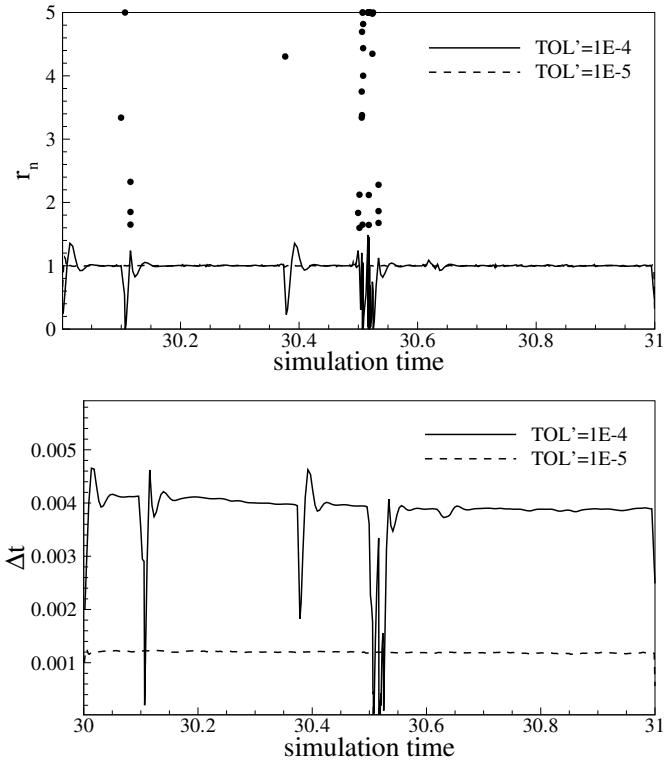

Figure 7: Cylinder. Evolution of the error estimator of the adaptive time-step strategy, r^{n+1}, (on the left) and of the time-step, Δt, (on the right) for adaptive peer3A scheme with $TOL' = 10^{-4}$ and $TOL' = 10^{-5}$, $TOL_{GMRES} = \eta TOL'$ and $\mathbb{P}^3$ solution approximation

schemes were used: ROS3PL for peer3 and peer4A, RODASP for peer5A and RODAS-ROD5_1 for peer6A.

The error on the lift coefficient, the computational time, the average time-step and the Courant-Friedrichs-Lewy number for different adaptive tolerances are reported in Tab. 6. Lower adaptive tolerance values can greatly increase the total number of the time-step and consequently the computational cost of simulations that thus can be beyond the available resources. For this reason very small adaptive tolerances, *i.e.* $TOL' = 10^{-7}$ and $TOL' = 10^{-8}$ for peer3A and $TOL' = 10^{-8}$ for peer4A, have not been considered in this work.

On the other hand, with higher adaptive tolerance values numerical instabilities appear, as depicted in Fig. 7, which shows the evolutions of the error estimator r^{n+1} and of the time-step for peer3A scheme ($TOL' = 10^{-4}$ and $TOL' = 10^{-5}$). The simulation with $TOL' = 10^{-5}$ is more stable, the error estimator slightly fluctuates around δ and there is no rejected time-step. Instead, the adaptive time-step strategy with $TOL' = 10^{-4}$ shows strong variations of the error estimator, leading to a high number of rejected time-steps, approximately 10%, and, as a consequence, to a higher computational cost. The origin of these instabilities could be related to the loss of the linearisation properties, an well known issue that can also affect Rosenbrock schemes.

As a consequence, optimal adaptive tolerances can be found for each Peer method: $TOL' = 10^{-4}$ for peer3A, $TOL' = 10^{-5}$ for peer4A and $TOL' = 10^{-7}$ for peer5A. Simulations with Peer6A have not been performed due to excessive computing time required by the small adaptive tolerance ($TOL' = 10^{-8}$), necessary to avoid numerical instabilities.

A performance comparison between the peer methods and the traditional one-step methods is shown in Figs. 8 and 9. As seen in the first test case, peer3A scheme must only be taken

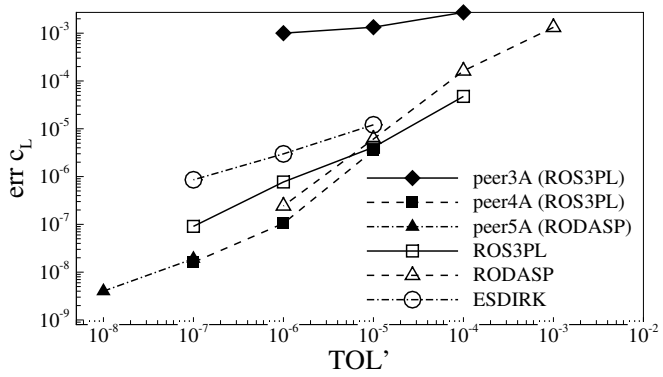

Figure 8: Cylinder. Error of the lift coefficient, err_{C_L}, as a function of the adaptive tolerance TOL' for adaptive Peer schemes, $TOL_{GMRES} = \eta TOL'$ and $\mathbb{P}^3$ solution approximation

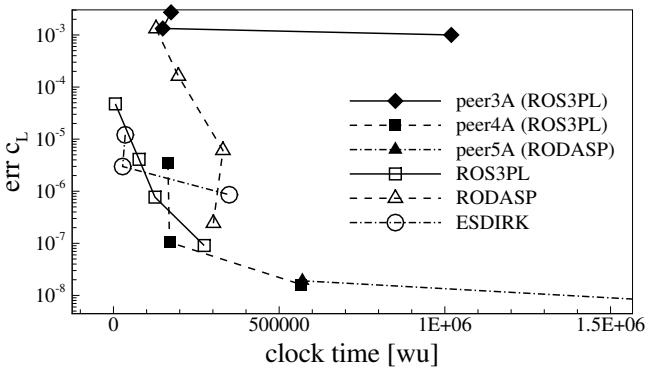

Figure 9: Cylinder. Error of the lift coefficient, err_{C_L}, as a function of the computational time for adaptive Peer schemes, $TOL_{GMRES} = \eta TOL'$ and $\mathbb{P}^3$ solution approximation

into account for very low level of accuracy, *i.e.* $err_{C_L} \geq 10^{-4}$. Instead, peer4A scheme with the optimal values of the adaptive tolerance TOL' is more efficient than ROS3PL scheme. Finally, because of numerical instabilities, peer5A scheme can become competitive in terms of efficiency only for very high accuracy, *i.e.* $err_{C_L} \leq 10^{-7}$

As in the previous test case, the tolerance calibration procedure can be used to reduce the difference in accuracy between time integration schemes. Calibration parameters are reported in Tab. 7.

5 Conclusions

In this work we have implemented the linearly implicit two-step Peer methods in a high-order discontinuous Galerkin solver for the numerical solution of incompressible unsteady flows. The performance, in terms of accuracy and computational efficiency, have been compared on laminar and turbulent test cases with one-step traditional methods.

The assessment showed different behaviours for the considered schemes depending on the flow regime of the test case, *i.e.* laminar or turbulent. On the laminar test case the Peer accuracy increases with the order of convergence leading to an efficiency improvement of time integration other traditional one-step implicit methods for high accuracy requirement. Instead, for the turbulent test case, even if Peer methods show a very high accuracy, their efficiency is comparable to Rosenbrock and ESDIRK ones.

Future works will assess Peer methods on other incompressible laminar and turbulent test

Table 6: Cylinder. Error of the lift coefficient, err_{C_L}, the average time-step Δt_{avg}, the average Courant-Friedrichs-Lewy number CFL_{avg}, the number of the rejected time-step [%] and the computational time for adaptive Peer schemes and different adaptive tolerance TOL', $TOL_{GMRES} = \eta TOL'$ and $\mathbb{P}^3$ solution approximation

	TOL'	err_{C_L}	Δt_{avg}	CFL_{avg}	% rejected time-step	CPU time [wu]
peer3A	1.00E-04	2.72E-03	2.95E-03	241.68	11.27%	1.73E+05
	1.00E-05	1.33E-03	1.19E-03	97.65	0%	1.48E+05
	1.00E-06	1.00E-03	3.77E-04	30.91	0%	1.02E+06
	1.00E-07	-	-	-	-	-
	1.00E-08	-	-	-	-	-
peer4A	1.00E-04	-	-	-	-	-
	1.00E-05	3.53E-06	3.12E-03	255.23	28.04%	1.64E+05
	1.00E-06	1.05E-07	1.70E-03	139.34	6.29%	1.69E+05
	1.00E-07	1.61E-08	7.03E-04	57.58	8.78%	5.67E+05
	1.00E-08	-	-	-	-	-
peer5A	1.00E-04	-	-	-	-	-
	1.00E-05	-	-	-	-	-
	1.00E-06	-	-	-	-	-
	1.00E-07	1.91E-08	1.09E-03	89.25	14.49%	5.70E+05
	1.00E-08	4.00E-09	4.24E-04	34.73	23.07%	2.50E+06

Table 7: Cylinder. Parameters for the calibration procedure

	k	β	TOL_0
peer3A	0.22	10^{-3}	10^{-6}
peer4A	1.17	9.55	10^{-6}
peer5A	0.68	5.24	10^{-7}

cases, to have a deeper understanding of their behaviour and performance, considering also time dependent boundary conditions, which can be handled by Peer schemes without order reduction. Furthermore, the coupling between DG method and Peer schemes will be evaluate also for compressible test cases.

Acknowledgements

HPC resources provided by CINECA within the "Convenzione di Ateneo Università degli Studi di Brescia" and "Convenzione di Ateneo Università degli Studi di Bergamo" are gratefully acknowledged.

REFERENCES

[1] D. N. Arnold, F. Brezzi, B. Cockburn, and D. Marini. Unified analysis of discontinuous Galerkin methods for elliptic problems. *SIAM J. Numer. Anal.*, 39(5):1749–1779, 2002.

[2] F. Bassi, L. Botti, A. Colombo, A. Crivellini, A. Ghidoni, and F. Massa. On the development of an implicit high-order Discontinuous Galerkin method for DNS and implicit LES of turbulent flows. *European Journal of Mechanics - B/Fluids*, pages –, 2015.

[3] F. Bassi, L. Botti, A. Colombo, A. Crivellini, A. Ghidoni, A. Nigro, and S. Rebay. Time Integration in the Discontinuous Galerkin Code MIGALE - Unsteady Problems. In Norbert Kroll, Charles Hirsch, Francesco Bassi, Craig Johnston, and Koen Hillewaert, editors, *IDIHOM: Industrialization of High-Order Methods - A Top-Down Approach*, volume 128 of *Notes on Numerical Fluid Mechanics and Multidisciplinary Design*, pages 205–230. Springer International Publishing, 2015.

[4] F. Bassi, L. Botti, A. Colombo, D.A. Di Pietro, and P. Tesini. On the flexibility of agglomeration based physical space discontinuous Galerkin discretizations. *Journal of Computational Physics*, 231(1):45 – 65, 2012.

[5] F. Bassi, L. Botti, A. Colombo, A. Ghidoni, and F. Massa. Linearly implicit Rosenbrock-type RungeKutta schemes applied to the Discontinuous Galerkin solution of compressible and incompressible unsteady flows. *Computers & Fluids*, 118:305 – 320, 2015.

[6] F. Bassi, A. Colombo, C. De Bartolo, N. Franchina, A. Ghidoni, and A. Nigro. Investigation of high-order temporal schemes for the discontinuous Galerkin solution of the Navier-Stokes equations. *11th World Congress on Computational Mechanics, WCCM 2014, 5th European Conference on Computational Mechanics, ECCM 2014 and 6th European Conference on Computational Fluid Dynamics, ECFD 2014*, pages 5651–5662, 2014.

[7] F. Bassi, A. Crivellini, D. A. Di Pietro, and S. Rebay. An artificial compressibility flux for the discontinuous Galerkin solution of the incompressible Navier–Stokes equations. *J. Comput. Phys.*, 218(2):794–815, 2006.

[8] F. Bassi, A. Ghidoni, A. Perbellini, S. Rebay, A. Crivellini, N. Franchina, and M. Savini. A high-order discontinuous galerkin solver for the incompressible RANS and $k-\omega$ turbulence model equations. *Computers & Fluids*, 98:54 – 68, 2014.

[9] F. Bassi, S. Rebay, G. Mariotti, S. Pedinotti, and M. Savini. A high-order accurate discontinuous finite element method for inviscid and viscous turbomachinery flows. In R. Decuypere and G. Dibelius, editors, *Proceedings of the 2nd European Conference on Turbomachinery Fluid Dynamics and Thermodynamics*, pages 99–108, Antwerpen, Belgium, March 5–7 1997. Technologisch Instituut.

[10] Andrea D. Beck, Thomas Bolemann, David Flad, Hannes Frank, Gregor J. Gassner, Florian Hindenlang, and Claus-Dieter Munz. High-order discontinuous Galerkin spectral element methods for transitional and turbulent flow simulations. *International Journal for Numerical Methods in Fluids*, 76(8):522–548, 2014.

[11] F. Brezzi, M. Manzini, D. Marini, P. Pietra, and A. Russo. Discontinuous Galerkin approximations for elliptic problems. *Numer. Methods Partial Differential Equations*, 16:365–378, 2000.

[12] Simmendinger C. and Versick D. Integrated performance analysis of computer systems (ipacs). benchmarks for distributed computer systems. *Praxis der Informationsverarbeitung und Kommunikation*, 28(3), 2005.

[13] M. H. Carpenter, C. A. Kennedy, Hester Bijl, S. A. Viken, and Veer N. Vatsa. Fourth-order Runge—Kutta schemes for fluid mechanics applications. *J. Sci. Comput.*, 25(1):157–194, October 2005.

[14] M.H. Carpenter, S.A. Viken, and E.J. Nielsen. The efficiency of high order temporal schemes. In *41st Aerospace Sciences Meeting and Exhibit*, 2003.

[15] C. Carton de Wiart, K. Hillewaert, M. Duponcheel, and G. Winckelmans. Assessment of a discontinuous Galerkin method for the simulation of vortical flows at high Reynolds number. *Int. J. Numer. Methods Fluids*, 74(7):469–493, 2014.

[16] J.-B. Chapelier, M. de la Llave Plata, F. Renac, and E. Lamballais. Evaluation of a high-order discontinuous Galerkin method for the DNS of turbulent flows. *Comput. Fluids*, 95(0):210 – 226, 2014.

[17] A. Crivellini, V. D'Alessandro, and F. Bassi. Assessment of a high-order discontinuous Galerkin method for incompressible three-dimensional Navier-Stokes equations: Benchmark results for the flow past a sphere up to Re=500. *Computers and Fluids*, 86:442–458, 2013.

[18] E. Fehlberg. Classical fifth-, sixth-, seventh-, and eighth-order runge-kutta formulas with stepsize control. *NASA TR R-287*, 1968.

[19] Gregor Gassner, Michael Dumbser, Florian Hindenlang, and Claus-Dieter Munz. Explicit one-step time discretizations for discontinuous galerkin and finite volume schemes based on local predictors. *Journal of Computational Physics*, 230(11):4232 – 4247, 2011. Special issue High Order Methods for {CFD} Problems.

[20] A. Gerisch, J. Lang, H. Podhaisky, and R. Weiner. High-order linearly implicit two-step peer - finite element methods for time-dependent pdes. *Applied Numerical Mathematics*, 59(34):624 – 638, 2009. Selected Papers from NUMDIFF-11.

[21] A. Ghidoni, E. Pelizzari, S. Rebay, and V. Selmin. 3D anisotropic unstructured grid generation. *Int. J. Numer. Meth. Fl.*, 51(9-10):1097–1115, 2006.

[22] Florian Hindenlang, Gregor J. Gassner, Christoph Altmann, Andrea Beck, Marc Staudenmaier, and Claus-Dieter Munz. Explicit discontinuous Galerkin methods for unsteady problems. *Computers & Fluids*, 61:86 – 93, 2012.

[23] J. Lang and D. Teleaga. Towards a fully space-time adaptive FEM for magnetoquasistatics. *Magnetics, IEEE Transactions on*, 44(6):1238–1241, June 2008.

[24] G. Di Marzo. *RODAS5(4)-Mthodes de Rosenbrock d'ordre 5(4) adaptes aux problemes diffrentiels-algbriques*. 1993.

[25] A. Nigro, C. De Bartolo, F. Bassi, and A. Ghidoni. Up to sixth-order accurate A-stable implicit schemes applied to the discontinuous Galerkin discretized Navier-Stokes equations. *J. Comput. Phys.*, 276(0):136 – 162, 2014.

[26] A. Nigro, A. Ghidoni, S. Rebay, and F. Bassi. Modified Extended BDF scheme for the discontinuous Galerkin solution of unsteady compressible flows. *Int. J. Numer. Methods Fluids*, 76(9):549–574, 2014.

[27] H. Podhaisky, R. Weiner, and B.A. Schmitt. Rosenbrock-type 'peer' two-step methods. *Applied Numerical Mathematics*, 53:409 – 420, 2005. Dedicated to Profesor Karl Strehmel, on the occasion of his 70th birthday.

[28] Gustaf Soderlind. Digital filters in adaptive time-stepping. *ACM Trans. Math. Softw.*, 29(1):1–26, March 2003.

[29] Gustaf Soderlind and Lina Wang. Adaptive time-stepping and computational stability. *Journal of Computational and Applied Mathematics*, 185(2):225 – 243, 2006. Special Issue: International Workshop on the Technological Aspects of Mathematics.

[30] F. Steinebach. Order reduction of ROW methods for DAEs and method of lines applications. *Techn. Hochsch., Fachbereich Mathematik*, 1995.

[31] Fedderik van der Bos and Bernard J. Geurts. Computational error-analysis of a discontinuous galerkin discretization applied to large-eddy simulation of homogeneous turbulence. *Computer Methods in Applied Mechanics and Engineering*, 199(1316):903 – 915, 2010. Turbulence Modeling for Large Eddy Simulations.

[32] Liang Wei and Andrew Pollard. Direct numerical simulation of compressible turbulent channel flows using the discontinuous Galerkin method. *Comput. Fluids*, 47(1):85 – 100, 2011.